Contribution of mask roughness in stochasticity of high-NA EUV imaging

Rik Jonckheere [1], Lawrence S. Melvin III [2]

[1] imec
Kapeldreef 75, B-3001 Leuven, Belgium
[2] Synopsys
2025 NW Cornelius Pass Road, Hillsboro, OR 97124, United States

ABSTRACT

This paper extends the 2019 and 2020 symposium contributions clearly showing that (local) mask defects and non-local mask defects (NLMDs) act as triggers for increased stochastic failure probability on the EUV printed wafer. The present work focuses on anamorphic imaging at 0.55 NA, including horizontal and vertical pattern orientations, and comprises defocus conditions and line breaking as a second failure mechanism. Two roughness type NLMDs are studied: multilayer (ML) ripple relates to a non-fully planar coating of the ML mask stack. Mask absorber line-edge roughness is addressed as a second roughness type NLMD. The longer-term intent is to inspire defining limits to their impact, from the perspective that an increased mask contribution to stochastics of high-NA EUV lithography must be avoided.

Keywords: EUV lithography, stochastic failures, EUV mask, mask specifications, mask roughness, multilayer mirror, line-edge roughness

1. Introduction

Application of extreme ultraviolet (EUV) lithography in the production of integrated circuits calls for attention to stochastic failures on wafer. These random pattern errors can be observed as bridges or breaks for line patterns, or as missing contacts or kissing contacts in contact hole layers [1]. An elevated frequency of such occurrence is incompatible with guaranteed manufacturing yields.

Previous work [2-4] showed that mask defectivity contributes to stochastics of EUV imaging on wafer. At first, imaging of 16nm lines and spaces (l/s) at a numerical aperture (NA) of 0.33 was studied. Local defects such as defects in the multi-layer (ML) mirror, absorber defects and particles were shown to display a universal behavior [2]. The printed critical dimension (CD) non-stochastic local deviation caused by the presence of such a defect directly determines the resulting pattern variability and failure probability, obtained in the approach of multiple stochastic simulations for the same situation. This holds equally true for the *average* CD deviation at the defect location, directly obtained in the latter. The stochastic simulations use different random seeds for the different contributing aspects of the stochastics of the imaging process, as will be explained further.

In a second step, it has been shown that non-local mask deficiencies (NLMDs) act the same manner [3]. An NLMD refers to a shortcoming of any aspect of mask quality, such as CD error, absorber slope, contamination growth, but also roughness. The only difference is that the NLMD's trigger to initiate stochastic failures on wafer is not localized around a defect site, but can occur anywhere where the mask quality is sub-optimal. Non-roughness type NLMDs, such as CD bias and absorber slope, have been shown to scale with the impact on the aerial image, or specifically with the normalized intensity log-slope (NILS). Roughness type NLMDs, such as ML-ripple and mask absorber line-edge roughness (LER), cause variation of the aerial image intensity across the mask pattern. ML-ripple is understood to cause a local variability of the ML reflectivity. Mask absorber LER refers to a medium-to-high frequency variation of the mask CD. Both effects were shown to cause a local variation of the printed CD, which occasionally can cause a failure such as line bridging or line breaking. This finding already earlier inspired to treat also the non-roughness type of NLMDs as a (low frequency) non-uniformity. Insufficient CD uniformity (CDU) of the mask means that locally in the total layout the mask CD will be too small or too large. Despite

this variation on mask, the exposure dose is chosen to obtain – on average – the targeted printed CD on wafer. Locations with too small or too large mask CD will cause a deviation of the printed CD on wafer, to an amount determined by the mask error enhancement factor (MEEF). The same is true in stochastic simulations and only requires that the statement is updated to an *average* deviation of the printed CD on wafer. An additional aspect is that, depending on the effective CD on wafer at a certain location, pattern failures can occur in the form of line breaking or – bridging [1]. In the present work we have therefore introduced the random nature of the effective mask CD to study its additional influence beyond that of roughness type NLMDs only, the latter having been the original intent of this work. In addition, a variation of focus (while not an NLMD, but another influencer of NILS), has equally been adopted. In the earlier work [3] wafer defocus had also been studied as an offset from best focus.

The present work addresses imaging of 11nm lines and spaces at 0.55NA EUV. This high-NA EUV imaging is anamorphic, as the magnification factor is different for the 2 axes of the mask pattern. While in the exposure slit direction the conventional 4x magnification is maintained, in the scan direction it is increased to 8x (for a recent update see Ref. 5). First work in this series on mask contribution to stochastics at 0.55NA [4] has studied the effect of local ML-defects to the printed result on wafer and showed a dependence on the orientation of the l/s pattern, either parallel to the scan direction ("vertical") or perpendicular to it ("horizontal"). Such difference could be expected, being hinted by the difference in magnification factor. While focusing on the center of slit, a typically lower failure probability was found for horizontal l/s, despite they are shadowed (in view of the chief ray angle of incidence), while vertical lines are not.

The present work extends this imaging study for 11nm l/s by means of 0.55NA EUV lithography, now addressing roughness type NLMDs, specifically ML-ripple and absorber LER.

2. Simulation conditions and methodology

With the details of the methodology and simulation conditions for mask, optical settings, resist process detailed in an earlier publication [6], just a summary is given here. Figure 1 illustrates the optical settings for the 0.55NA scanner, showing the central obscuration in the projection optics and the selected leaf-shaped dipole source optimized for 11nm l/s. Of specific relevance is the anamorphic nature of imaging (not shown), through which the results of orienting the l/s pattern either in the 8x scan direction or the 4x slit direction, can be expected to differ.

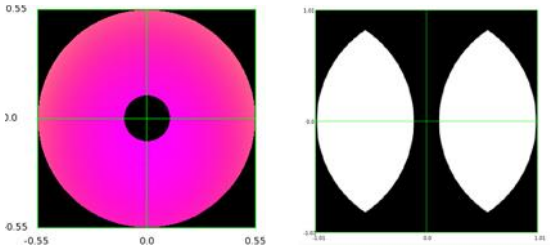

Figure 1: Optical settings for 0.55NA; (left) pupil of projection optics with central obscuration, (right) leaf-shaped dipole illumination optimized for 11nm l/s pattern (shown for vertical orientation).

While the selected optical conditions are set to represent the ASML EXE5000 0.55NA system, for resist patterning an artificial resist model has been used. It is shown to predict trends in which mask aspects are expected to contribute to the stochastics of the printed image on wafer [6]. The model intentionally triggers an increased wafer defectivity, and therewith gives an overestimation compared to resist processes used in fabrication. This overestimation facilitates investigating mask influences in small simulation areas (on the order of 1 μm^2) within manageable simulation time.

The model applied for the exposure of resist consists of seven stochastic phenomena:

- Photon shot noise, by means of secondary electron distribution
- Inhibitor distribution
- PAG (photo acid generator) distribution
- PAG activation
- Quencher distribution
- Quencher deactivation
- Post-exposure bake kinetics

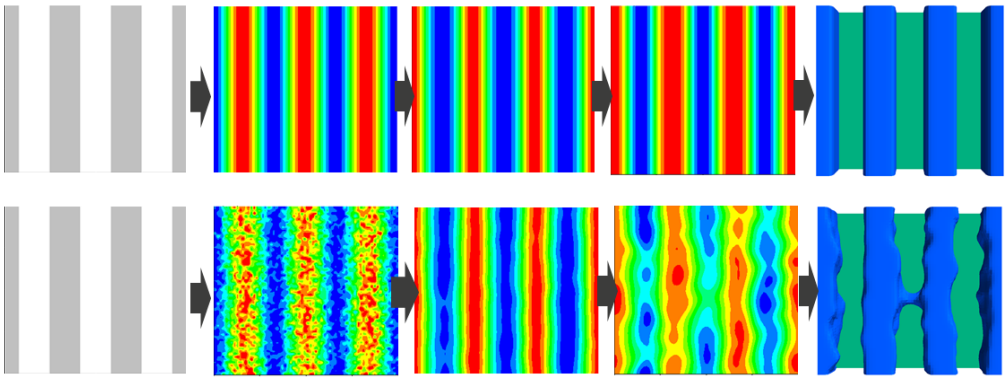

Figure 2: Visualization of the randomized events for a stochastic approach (bottom row) compared to a continuum model, where each aspect is characterized by a fixed numerical value (top row). Subsequent calculation steps, and obtained distribution of the comprised aspects, are (from left to right, in top view), an ideal mask pattern (shown at 1x wafer scale here), the aerial image intensity due to shot noise, the PAG concentration, the degree of inhibitor protection and the obtained patterned resist.

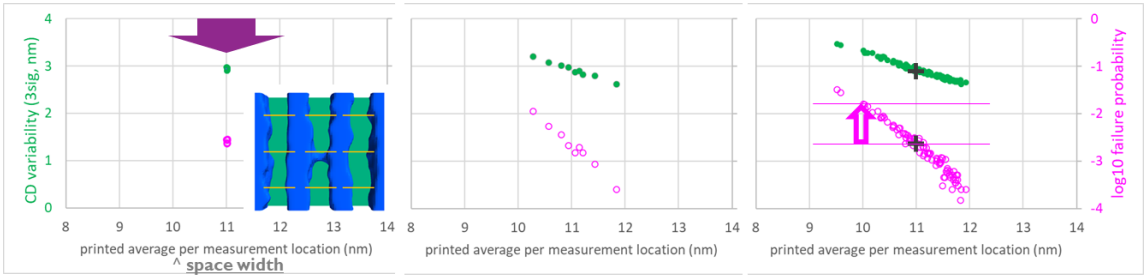

Figure 3: Methodology of plotting both CD variability and failure probability as a function of printed space width. For a perfect mask (left), all metrology sites (nine shown across the obtained top view in resist, see the inset) provide an identical result. For a mask with a roughness type NLMD, simulated with just one random seed, a spread in the printed CD is already observed across the nine measurement positions (center). This spread increases as the simulation is repeated with more random inputs for the substrate roughness, for the same parameters L_c and RMS (right). The variation of the printed CD triggers a varying, but overall increasing, failure probability (as shown by the arrow at the target CD - 10% value).

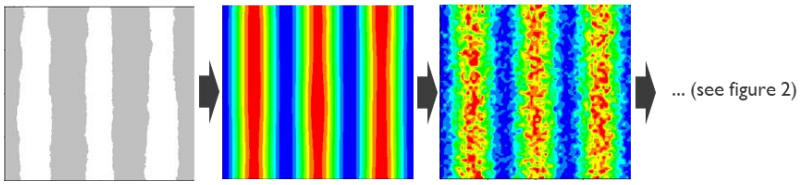

Figure 4: Visualization of the effect of an imperfect mask with a roughness-type NLMD. The most right-hand stage corresponds to the second stage of the bottom row in figure 2. It illustrates that the non-perfect mask (left, with absorber LER as example) by itself becomes the first stage of random variation. The center panel illustrates the amount of aerial image intensity variation due to the mask itself in a non-stochastic situation. The right panel additionally includes shot noise as the first step of the stochastic resist exposure model used. Subsequent aspects are as included in figure 2, but those can be expected to display larger variation (not shown).

Random seeds were applied to each of these aspects. Each seed sets a different value within the defined uncertainty of the aspect. Repeating this over typically twenty thousand runs, a variation in the resulting resist image on wafer is obtained. Figure 2 illustrates this different approach of a stochastic model compared to a conventional continuous approach.

The obtained resist image is analyzed at a number of measurement positions, as indicated in figure 3. After dose tuning to obtain an average printed target space width of 11nm from 20000 random runs, one determines the three-sigma CD variability and also counts the number of lines bridging events [footnote 1]. While the explanation of figure 3 is for a "perfect" mask and therefore provides identical results for each measurement position (within error flag), the goal for this work is to assess how these results are affected by use of a non-perfect mask that exhibits one or more NLMD(s). This work concentrates on roughness type NLMDs.

As the mask displays a certain roughness, an updated version of figure 2, shown in figure 4, reflects that the mask already causes a variation in aerial image intensity "prior to" adding the shot noise effect or any other stochastic effect listed above (and illustrated through figure 2). Further variation can be observed in the subsequent aerial image including shot noise.

Figure 3 illustrates the spread of the obtained printed wafer space width across nine measurement positions when additional stochastic ML ripple cases are added. As the corresponding CD variability and failure probability show a strong correlation to the printed space width, an important down-side of this CD spread is that the number of stochastics failures for undersized space width is increased up to an order of magnitude, causing a net increase compared to a perfect mask.

The graphing formats in figure 3 have been applied to the investigation of the mask roughness contribution to stochastic failures in the following section. More spread is caused as roughness increases. Note that further in the discussion (especially on absorber roughness) the aerial image intensity prior to shot noise calculation, as included in figure, 4 has been used. However, only one such image provides rather qualitative impressions. Although possible, no equally massively quantitative results have been derived.

3. Results and discussion

3.1 ML-ripple

As a reminder, the approach taken to study ML-ripple and the corresponding representation is adopted here from Ref. 3 as figure 5.

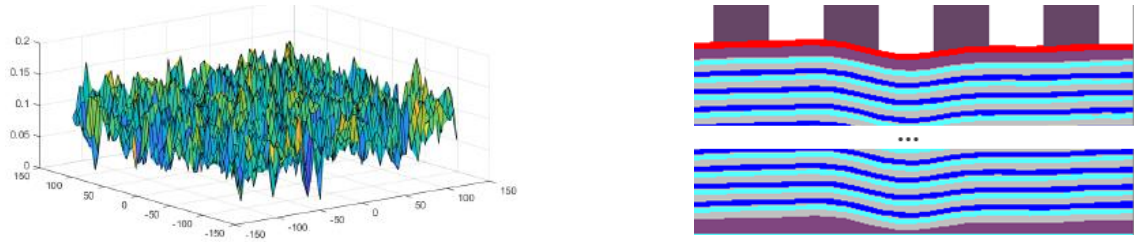

Figure 5: (adopted from Ref. 6) ML-ripple is simulated as substrate surface roughness (left), combined with unsmoothed ML deposition (right). The illustrative example for substrate roughness is for 100pm RMS (at 4x), corresponding to a peak-to-valley range of about 0.72nm (4x), which amounts to ~10% of the typical ML period. Equally the illustration for conformal deposition corresponds to a correlation length of 100nm at 4x.

With the methodology to emulate ML ripple explained in Ref. 6, its two main variables are the RMS value (root-mean-square of the amplitude) and the correlation length L_c.

[1] In the appendix it is explained why this work has focused on line bridging and did not include line breaking.

Figure 6 gathers the results obtained for a variation of L_c, while keeping a fixed value of 12.5pm RMS at 1x. As L_c is increasing, the CD spread around the 11nm target space width is increasing and appears to saturate near the largest value studied. The obtained results show that this CD spread is larger for vertical orientation of the l/s pattern, compared to horizontal. As the correlation length increases the background intensity in the pupilgram is shown to elevate.

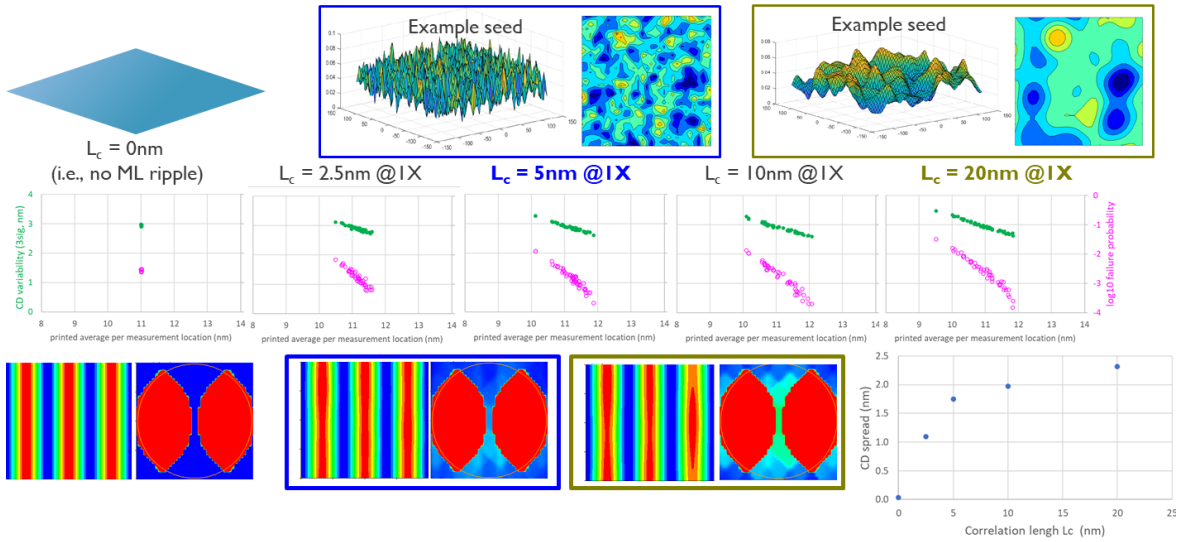

Figure 6: Investigation of ML-ripple at fixed RMS value of 12.5pm 1x, for a variation of correlation length L_c. Top row is a visualization of the initiating substrate surface roughness (both in perspective view and by means of a contour plot), for two instances corresponding to the color coding applied in the second row, showing the stochastic results (in the format of figure 3). As the obtained CD spread increases as L_c increases, also the background intensity in the pupil (bottom row) is increased. The relation between the obtained CD spread and L_c is plotted bottom right for both horizontal and vertical pattern orientation. Note that the pupilgrams are shown for a low maximum intensity as to better visualize the increasing background intensity as compared to that caused by the diffraction pattern of the l/s pattern.

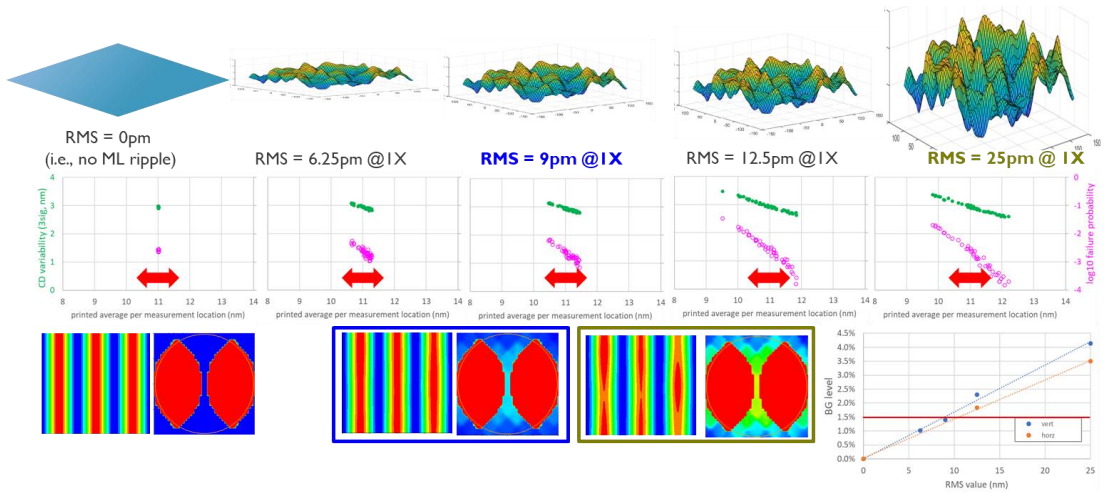

Figure 7: Investigation of ML-ripple at fixed value for correlation length L_c at 20nm 1x, for a variation of RMS. Top row is a visualization of the initiating substrate surface roughness (in perspective view). The second row shows the stochastic results (in the format of figure 3). As the obtained CD spread increases as RMS increases, also the background intensity in the pupil (bottom row, at maximum intensity corresponding to that in figure 6) is increased. The relation between this background level and RMS is plotted bottom right for both horizontal and vertical pattern orientation. The marked level of 1.5% is defined as acceptable and corresponds to a selected acceptable CD spread (marked by the red arrows) of ±0.5nm (see further).

Such is also apparent from the results studying a variation of the RMS value at a fixed L_c of 20nm at 1x (shown in figure 7). The resulting CD spread becomes excessive as it already exceeds a typical +/-10% tolerance. A linear behavior of the background intensity level in the pupilgram with RMS is found. Based on these obtained results an acceptable CD spread of ±0.5nm has been defined, which corresponds to a background level of 1.5% compared to the intensity of the diffraction pattern of the l/s pattern itself.

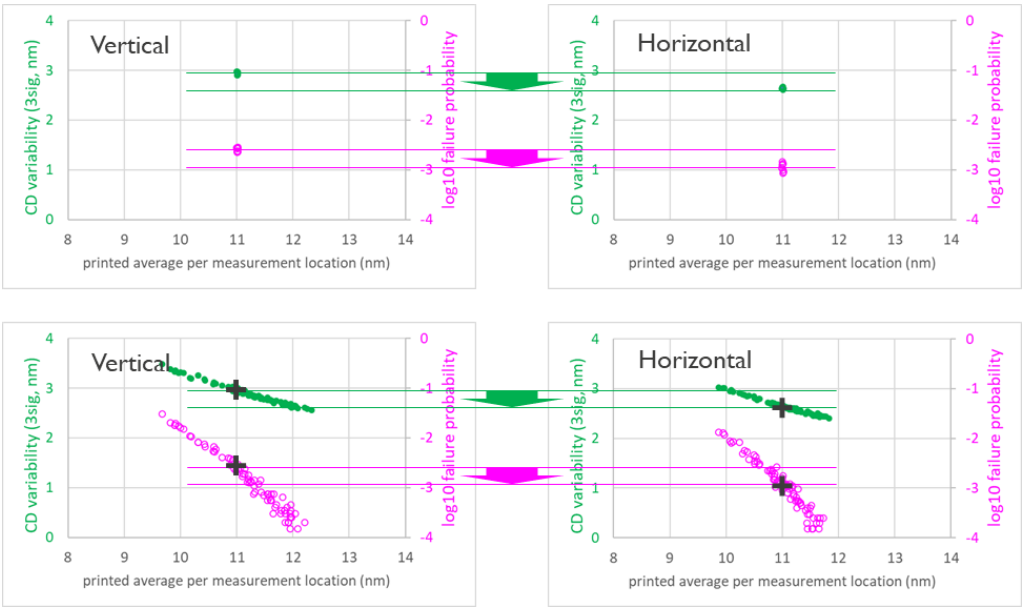

Figure 8: Illustration (by means of the format of figure 3) that the horizontal orientation for the same roughness situation display a smaller CD variability and failure probability, compared to vertical. Shown for perfect mask (top row) and ML-ripple with 12.5pm RMS and 20nm L_c (at 1x)

The present discussion owes an explanation why ML-ripple parameters RMS and L_c are mentioned at 1x throughout this document. All mask inputs into the simulator are given at 1x. For RMS, a 12.5pm value at 1x is correctly representing 50pm RMS value at mask. This value can be considered representing state-of-the-art [7]. In view of the anamorphic imaging (with 4x magnification in X direction and 8x in Y), defining L_c at wafer scale, effectively meant that in mask dimensions, as used for calculation, it is twice larger in Y (scan direction) compared to X (slit direction). Regardless, and as the shown simulation results are obtained for center-of-slit, which means that horizontal lines are shadowed unlike vertical lines, the obtained results show that the horizontal orientation of the l/s pattern gives lower values for CD variability and failure probability, as shown in figure 8. Also the obtained spread (on x-axis of the graph) in printed CD is found smaller for horizontal direction. This smaller mask influence for horizontal orientation is understood due to its higher NILS. Because of the asymmetric translation of the 1x input, it was preferred to continue to report all mask parameters as 1x throughout this document, except where explicitly mentioning them at mask scale. Mask roughness parameters in z-direction (i.e., perpendicular to the pattern plane) at mask need to be multiplied by 4. Those in the pattern plane need to be multiplied by 4 for slit direction (X) and 8 for the scan direction (Y).

3.2 Effect of defocus and mask CDU error

In this paragraph a suggestion is addressed that was received during the review process of Ref. 6, i.e., how focus variation influences the earlier findings. In general, in correlation with NILS deteriorating in defocus conditions, an increase of CD variability and failure probability was found when working at a defocus offset, while still retargeting the exposure dose. In this case, a variation of defocus (0, ±5nm, ±10nm) is applied to the stochastic process and that caused by mask ML-ripple (as covered in the previous paragraph), while applying the same exposure dose as for the best focus, the results of figure 9 are obtained. Such focus offset keeps the spread of average printed space width (horizontal axis of the graph) identical, but

the range for CD variability and failure probability as a result of focus variation widens towards larger values (vertical axis). A variation of focus across +/10 nm causes an overall limited effect.

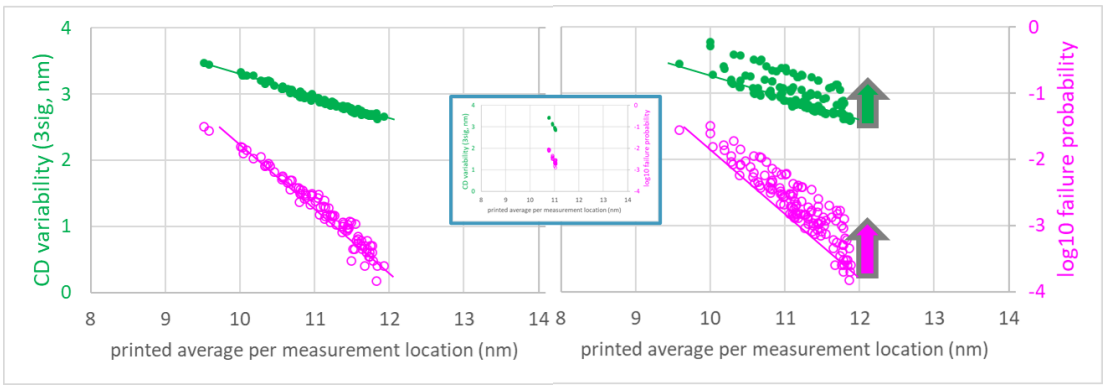

Figure 9: Illustration (by means of the format of figure 3) for the effect of defocus (shown for vertical orientation). (left) ML-ripple with 12.5pm RMS and 20nm L_c (at 1x) exposed at best focus; (right) corresponding superposed results for 5 focus settings (0, ±5nm, ±10nm); (inset) superposed results for the same 5 focus settings, but for mask without ML-ripple.

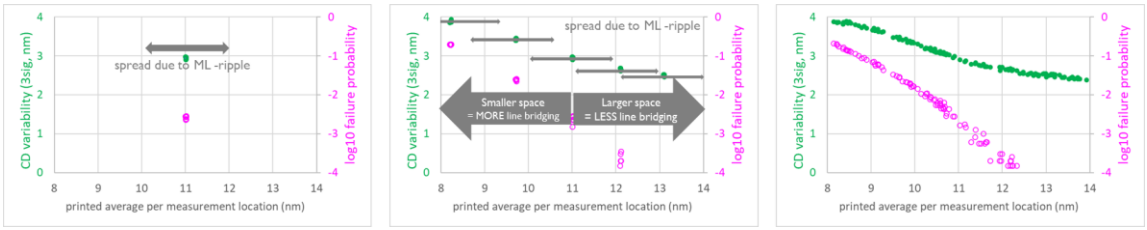

Figure 10: Illustration for the effect of CD uniformity error (shown for vertical orientation). (left) perfect mask with the arrow indicating the CD spread caused by ML-ripple with 12.5pm RMS and 5nm L_c (at 1x); (center) superposed results for mask without ML-ripple, yet with varying effective mask "bias" of (0, ±0.5nm, ±1nm at wafer scale), all exposed at the dose determined by bias 0, with the same CD spread marked for each result; (right) emerging result for simultaneous mask CD variation and said ML-ripple.

In similar ways one of the earlier treated NLMDs [3] was re-addressed. A small CD error, actually a CD mean-to-target error, while causing just limited change in NILS, did not significantly impact CD variability, nor failure probability. Yet this finding assumed that re-optimization of the exposure dose was possible to obtain on-target CD on wafer. The present work readdressed this from the approach that the CD error is rather a CD uniformity error, in which there is variation of the actual CD across the mask, with an average still on target and determining the dose-to-size applied for all deviating CDs across the mask.

It was found that a mask CD uniformity error has a massive impact in addition to that of ML-ripple, as shown in figure 10. Locations where the mask CD is too small or too large will print too small, or too large, on wafer, to an amount determined by the MEEF of the imaging process. For each of the locations there is a CD spread around the obtained value, due to of ML-ripple. The net massive spread of the printed CD comes with a huge variation of failure probability as determined by the obtained space width, as already explained in figure 3, but here it even exceeds three orders of magnitude. Specifications for ML ripple and CDU must for each be defined in a way conscious of the other. The example in figure 10 demonstrates that stochastic modeling asks for tighter mask specifications, due to the cumulative impact of multiple NLMDs.

3.3 Mask absorber LER

As a further roughness type NLMD, this paragraph studies mask absorber LER. This is a high frequency version of mask CD non-uniformity. It is parametrized [6] by a σ_{LER} (amplitude), a correlation length L_c and α is a unitless roughness exponent, the latter of which in our work was fixed to 0.5. A first set of parameters has shown a large impact of absorber

LER that manifests itself the same way as found for ML ripple (compare figure 11 to figures 6 and 7). The selected parameters clearly cause a variability and failure probability that exceeds what can be tolerated. These results for mask LER, while extreme, together with previous coverage of combined ML-ripple and CDU, again warn for the cumulative effect of several NLMDs, a point that is addressed further-on.

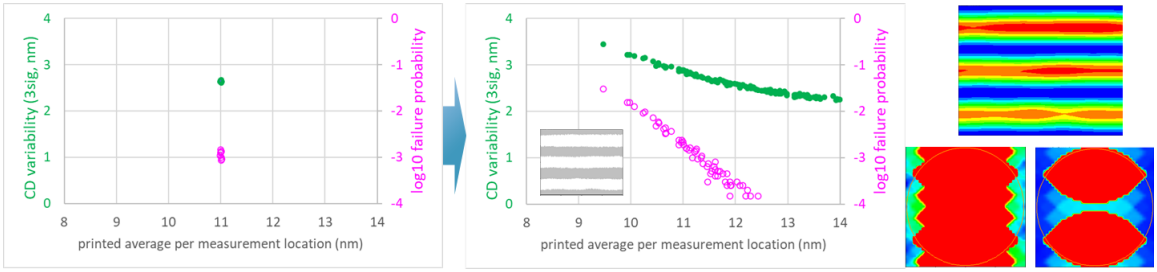

Figure 11: Illustration for the effect of absorber LER (shown for horizontal orientation). (left) reference for a perfect mask; (center) stochastic result for (α, σ_{LER}, L_c) = (0.5, 0.625nm, 20nm) @1x, visualized in the inset; (top right) impact on aerial image intensity (prior to shot noise calculation) of said absorber LER; (bottom right) corresponding pupilgram showing increasing background intensity (left of 2 panels is for the same maximum intensity as applied in figures 6 and 7, right of 2 panels is for an increased value thereof, as to still distinguish that of the imaged diffraction orders for the l/s pattern.

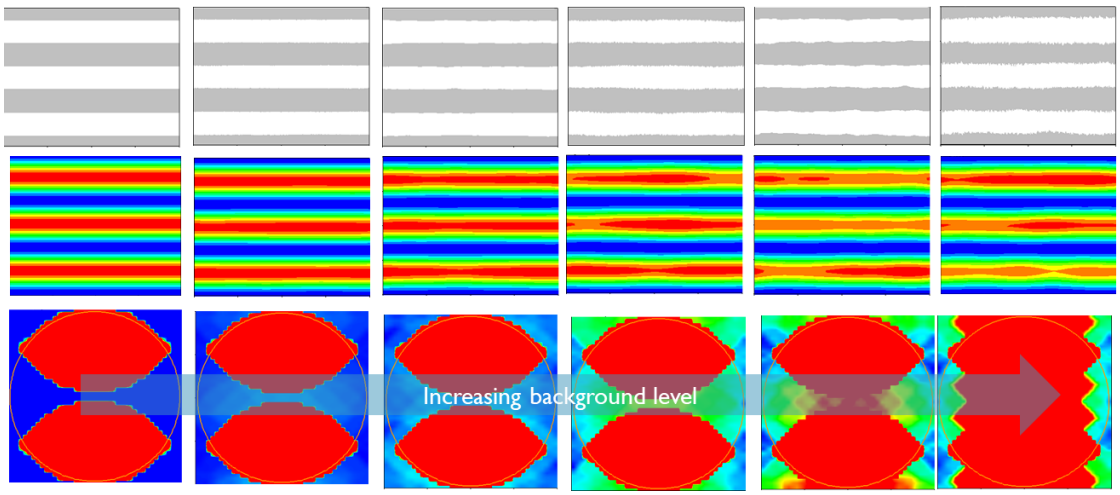

Figure 12: Effect of absorber LER for increasing σ_{LER} (from left to right from 0 to 0.625nm in increments of 0.125nm) at (α, L_c) = (0.5, 20nm) @1x. (top row) mask top view for a selected random seed, (center row) corresponding aerial image prior to calculation of shot noise, (bottom row) pupilgram at maximum intensity corresponding to that in figures 6 and 7.

The obtained results also illustrate that the printing impact of mask LER can again be explained by an increased background intensity in the pupilgram. No detailed study of stochasticity for varying LER parameters was undertaken. Moreover, while of interest, a combination of roughness-type NLMDs is found very calculation intensive. Instead, correlating further to the background level in the pupilgram proved useful, as now further discussed.

Figure 12 illustrates mask absorber LER for increasing σ_{LER} at a fixed value of L_c of 20nm (1x). From 0.375nm (1x) onwards it has a clearly visible impact in the aerial image (prior to shot noise effect calculation). From this level onwards the background intensity level in the pupilgram has become a larger percentage of that of the overlapping (0 and 1) diffraction orders of the 11nm hp pattern. Figure 13-left plots this background level as a function of σ_{LER}. A different sensitivity to absorber LER is found for horizontal and vertical orientation. Reapplying the value of 1.5%, derived for ML-ripple in figure 4, as acceptable relative background intensity, reveals a tolerance for mask σ_{LER} of ~0.11nm (1x) for V and ~0.17nm for H. Figure 13-right plots the background intensity level as a function of L_c. As also found for ML ripple, the influence of a certain sigma value saturates from a value for L_c above 10nm.

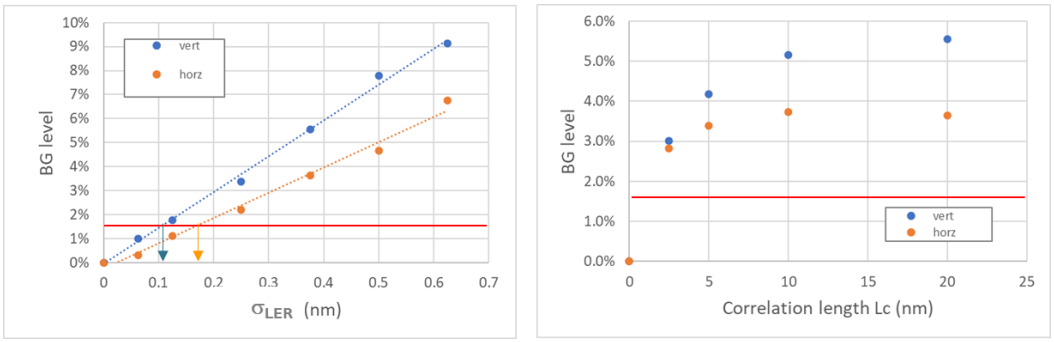

Figure 13: Background intensity in the pupil for varying absorber LER parameters, for two orientations of the l/s pattern. (left) as a function of σ_{LER} at fixed L_c = 20nm; (right) as a function of L_c at fixed σ_{LER} = 0.375nm.

3.4 Combination of ML-ripple and absorber LER

In a further step the combination of ML-ripple and absorber LER is studied, as to propose a methodology to generate mask specifications for these roughness type NLMDs, and how to define such in addition to already established specifications, such as for CDU. In figure 14 the results in figure 13-left for vertical orientation are repeated and complemented with what they become if in addition to absorber LER, ML-ripple is added as a contributing NLMD. The other panels in figure 13 illustrate 2 selected combinations, as marked by arrows, in how their aerial image and their background intensity in the pupilgram are affected.

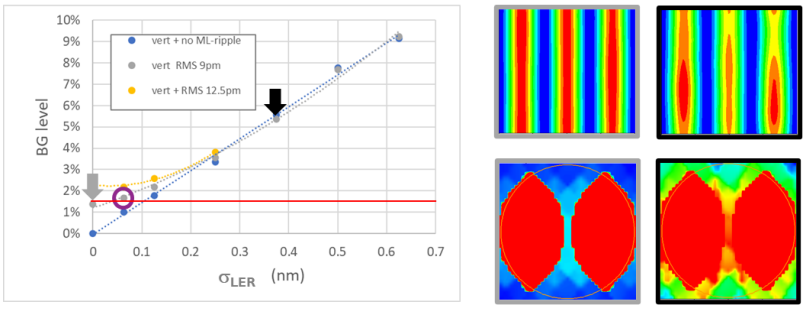

Figure 14: Background intensity in the pupil as a function of σ_{LER} (cfr. vertical orientation in figure 13), with additional ML-ripple with shown RMS and a $L_{c,MLR}$ of 20nm (1x). For 2 cases in the graph indicated by the grey-tone arrows, the right panels illustrate the aerial image variation, prior to shot noise calculation (top) and pupilgram (bottom) with same maximum intensity values as in figure 6, 7, 12.

Together with the corresponding panel in figure 4 for 9pm RMS ML-ripple, the circled combination in figure 14 with absorber LER of 62.5pm (1x) is found close to satisfying the 1.5% maximum background intensity level that was derived in Section 3.1 for ML-ripple. It allows for a spread of the target printed CD of 11nm on wafer of ± 0.5nm. An equal tolerance can be assigned to mask CD uniformity, to the extent dictated by the MEEF of the imaging process. This example illustrates a methodology to constrain mask CDU, ML-ripple, and absorber LER. This can keep the obtained CDU on wafer within a set tolerance (typically ±10%, also applied here), and thereby keep the corresponding probability for line bridging under control. It is possible that future users of this proposed methodology will distribute the individual tolerances differently and make the acceptable increase of failure probability even tighter.

4. Conclusions and outlook

This study calls attention to the cumulative impact of NLMDs at 0.55NA, such as mask roughness and CD non-uniformity. Each individual NLMD causes an increased CD variability and failure probability on the printed wafer. In addition, they reinforce each other's impact. This requires high-NA mask specifications for roughness type NLMDs. A proposal was

made to define those in conjunction with the contribution of mask CD uniformity error, through the use of a pupil fill background scatter criterion.

The (artificial) resist model used in this work has been previously shown to predict defectivity and CD trends [6], although the obtained CD spread results are not calibrated to printed wafer results. Therefore, this work cannot provide quantitative specifications, but rather trends and relative estimations. With this caveat, from the point of view of mask contribution to stochastics of imaging, a ML-ripple RMS value of 50pm at mask level (assumed state-of-the art) is too high. The same is claimed for absorber LER with a σ_{LER} of 1nm on mask.

In this simulation study, both horizontal and vertical oriented l/s patterns were examined. The obtained results, for the center of the exposure slit, clearly show an orientation dependence of the mask contribution to the stochastic performance of high-NA EUV lithography. Failure probability on wafer is found approximately 50% lower for horizontally oriented patterns.

As an outlook to further work, an extension into 2D patterns, i.e., Tip-to-Tip structures (T2T), can be announced [9].

Acknowledgements

Simulations in this presentation were undertaken with Sentaurus Lithography EUV. The authors are grateful to Ulrich Klostermann and Yudhi Kandel of Synopsys, and Eric Hendrickx, Peter De Bisschop, Koen d'Havé, Vicky Philipsen, Jörn-Holger Franke of imec.

References

1 Peter De Bisschop "Stochastic printing failures in extreme ultraviolet lithography," Journal of Micro/Nanolithography, MEMS, and MOEMS 17(4), 041011 (25 September 2018); https://doi.org/10.1117/1.JMM.17.4.041011

2 Rik Jonckheere, Lawrence S. Melvin III, and Renzo Capelli "Stochastic printing behavior of ML-defects on EUV mask", Proc. SPIE 11147, International Conference on Extreme Ultraviolet Lithography 2019, 111470P (24 October 2019); https://doi.org/10.1117/12.2538153

3 Rik Jonckheere, Lawrence S. Melvin III "Stochastic printing behavior of non-local mask deficiencies in EUV lithography", Proc. SPIE 11517, Extreme Ultraviolet Lithography 2020; 1151710 (2020) https://doi.org/10.1117/12.2572998

4 Lawrence S. Melvin III, Rik Jonckheere, "Two-dimensional feature stochastic printing with mask deficiencies in high-NA EUV", Proc. SPIE 11609, Extreme Ultraviolet (EUV) Lithography XII; 116091S (2021) https://doi.org/10.1117/12.2584775

5 Jan Van Schoot, Sjoerd Lok, Eelco Van Setten, Ruben Maas, Kars Troost, Rudy Peeters, Jo Finders, Judon Stoeldraijer, Jos Benschop, Paul Graeupner, Peter Kuerz, Winfried Kaiser, Thomas Stammler "High-NA EUV lithography exposure tool: key advantages and program progress", Proc. SPIE 11609, Extreme Ultraviolet (EUV) Lithography XII; 1160905 (2021) https://doi.org/10.1117/12.2583640

6 Lawrence S. Melvin, Rik Jonckheere, "Contribution of mask defectivity in stochastics of EUVL-based wafer printing", J. of Micro/Nanopatterning, Materials, and Metrology, 20(2), 021003 (2021); https://doi.org/10.1117/1.JMM.20.2.021003

7 Patrick Naulleau, Yow-Gwo Wang, Tom Pistor "Extreme ultraviolet mask roughness effects in high numerical aperture lithography", Appl. Opt. 57(7), 1724–1730 (2018); https://doi.org/10.1364/AO.57.001724

8 Peter De Bisschop, Eric Hendrickx, "Stochastic printing failures in EUV lithography", Proc. SPIE 10957, Extreme Ultraviolet (EUV) Lithography X; 109570E (2019) https://doi.org/10.1117/12.2515082

9 Lawrence S. Melvin, Rik Jonckheere, "Mask Roughness Impact on Two Dimensional Features Imaged with High NA EUV Lithography", submitted for SPIE Advanced Lithography 2022

APPENDIX

Here it is explained how to situate the shown results relatively to the patterning cliffs of the stochastic failure window [1].

De Bisschop [1,8] has shown that imaging in EUV can cause stochastic failures in the form of bridging lines and breaking lines (see left panel of figure A1). Plotting their probability as a function of the printed space width, two so-called patterning cliffs appear. Between them, there is typically a process window with a more acceptable number of failures. That is referred to as the defect floor. Here, the true numbers are difficult to discover as a massive set of inspection data needs to be acquired.

All figures in this manuscript showing the contribution of mask defectivity to stochastics of the printed wafer are of the type shown in the right panel of figure 3. The range of printed space width applied appears to only visualize the line bridge cliff, despite holding the target CD within this range. The authors think this may be a side effect of the artificial resist model used, which as intended [6], increases the defectivity in a way that the number of simulations to visualize trends remains realistic and manageable. It is believed that tweaking the resist parameters may have shifted the process window between those patterning cliffs to the range of larger printed space width.

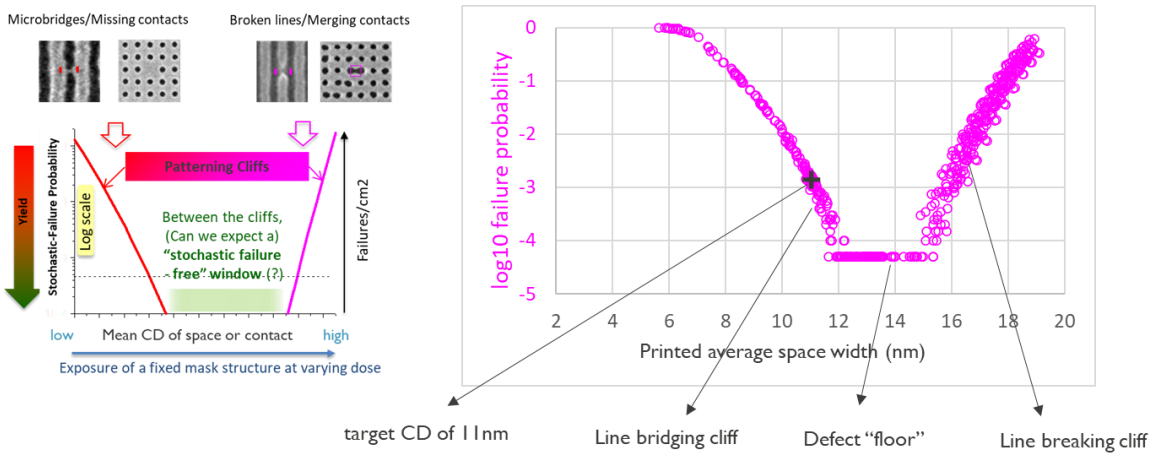

Figure A1: Patterning cliffs for broken lines and bridging lines as published by De Bisschop [8] (left). Extrapolating the range of printed CD in our work (in which only the bridging lines cliff was apparent) by explicit overexposure, has revealed the broken line cliff. In our simulation work the defect floor is defined as 0 detections in 20000 runs and artificially plotted here as 1 in 20000, in view of the logarithmic scale. Why the broken line cliff on the right appears wider is not yet understood. These results are obtained for ML-ripple with RMS 25pm and L_c 20nm (at 1x), an oversized space width of 12nm (at 1x) and several exposure doses all providing an average printed CD above the 11nm target. For none of the assessed NLMD's, even at extreme values (see Sct. 3), was the broken line cliff appearing at the applied dose-to-size.

To support this tentative explanation, a simulation has been undertaken for ML-ripple and oversized space width on mask, at considerably higher dose. Then, the obtained space width becomes very oversized on wafer and the residual resist line becomes very narrow. It is in these circumstances that broken lines starts to appear in the stochastics simulations of the present work, as shown in the right pane of figure A1. Hence, even with this artificial resist model, both patterning cliffs have been demonstrated present for a pitch of 22nm.